Letters

IOP Publishing

Plasma Sources Science and Technology

Plasma Sources Sci. Technol. **29** (2020) 03LT01 (7pp)

https://doi.org/10.1088/1361-6595/ab7087

Letter

Emerging and expanding streamer head in low-pressure air

T Hoder[1,2], Z Bonaventura[2], V Prukner[1], F J Gordillo-Vázquez[3] and M Šimek[1]

[1] Institute of Plasma Physics v.v.i., Department of Pulse Plasma Systems, Academy of Sciences of the Czech Republic, Prague, Czech Republic
[2] Department of Physical Electronics, Faculty of Science, Masaryk University, Brno, Czech Republic
[3] Instituto de Astrofísica de Andalucía (IAA-CSIC), Glorieta de la Astronomía s/n, Granada, Spain

E-mail: hoder@physics.muni.cz

Received 7 October 2019, revised 17 January 2020
Accepted for publication 27 January 2020
Published 4 March 2020

Abstract

The emergence of a streamer from an ionisation wave and its expansion are ultra-fast processes shaping the very first moments of the streamer development, and are usually accessible only by complex numerical models. In this Letter, we report experimental evidence of the emergence of a streamer from an ionisation wave in 1.3 kPa air, a laboratory analogue of early-stage streamers emerging in geophysical Blue Starters and Jets. The radially and temporally resolved electric field patterns of an expanding streamer are determined by sub-nanosecond optical emission spectroscopy. As the emerged streamer expands, the electric field decreases by a factor of 1.4 in 1 ns. We quantify the radial expansion of the streamer head and its axial acceleration, reaching the velocity of 10^7 m s^{-1}. In combination with electrical measurements, the transferred charge, electron density, and mean electron energy are quantified, enabling detailed insight into this ultra-fast phenomenon at its characteristic time-scale.

Keywords: streamer, electric field, low-pressure air, electron density, blue jet, transient luminous events, ionisation wave

Ionisation in atmospheric air frequently takes the form of contracted discharge filaments ruled by the streamer mechanism [1–6]. Streamers are ultra-fast contracted ionisation waves of enhanced electric field producing high-energy electrons and excited and ionised species [7]. Electron driven processes then change the chemical composition of the gas around the running streamer head. This fact is of crucial importance anywhere the streamer mechanism occurs: ozone generation and surface treatment using barrier and corona discharges [8, 9], as well as the plasma chemistry generated by streamers in lightning or in transient luminous events (TLEs, i.e. Sprites, Blue Starters and Jets etc) [10–12]. A profound understanding of the effects of atmospheric electricity [10, 12–14] or of the streamer-induced air chemistry in various applications [8, 15] relies on a detailed knowledge of the magnitude of the electric field in the streamer head.

While the quasi-stationary phase of the development of a non-branching streamer in free space is a well understood phenomenon (e.g. [16–19]), the very first stages of the initiation of the streamer in pulse driven/triggered discharges is still an unresolved issue. The general mechanism of the emergence of a streamer from a local instability or irregularity in the effective ionisation rate (due to perturbations in the background electron density or electric field redistribution) is an important issue for the physics of transient laboratory discharges [8, 20–23] as well as for electrical phenomena in the upper atmosphere [24–28]. Different models describe various effects and propose solutions which have not been validated experimentally. This is due to the typically high velocity of the streamer and to its erratic appearance, both in upper atmosphere luminous events as well as in large scale ozone generators or plasma treatment devices in the laboratory. Both theoretical [7, 17, 18, 20, 29, 30] and experimental

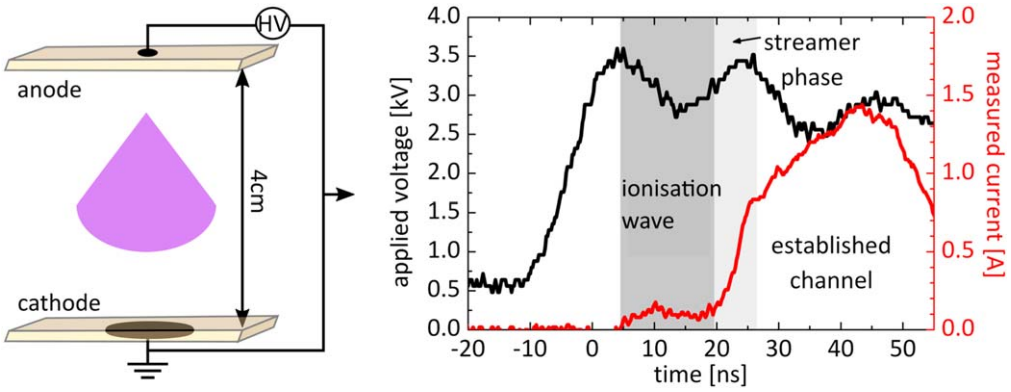

Figure 1. Simplified scheme of the experimental setup (left) and the measured electrical parameters in the external circuit.

[19, 21, 31–33] efforts have been made to understand this extremely fast ionisation process and to describe its development by the quantification of the electric field under different conditions. However, its detailed analysis from the initial conditions to the self-generated electric field enhancement in the contracted streamer head and its expansion remains mainly theoretical [20, 26, 34–36]. For example, Luque *et al* [26], Liu *et al* [37, 38] and others have theoretically shown that a downward-propagating ionisation wave collapses into a Sprite streamer as it propagates farther down under conditions in the lower ionosphere. We believe that the laboratory analogues of streamers in such discharges, as presented here, are of great interest for a deeper understanding of the studied phenomena.

In lower pressure pulse-initiated discharges, the ionisation starts with an initial diffuse ionisation cloud rapidly being transformed into an ionisation wave propagating with velocities lower than a typical streamer velocity [22, 26, 39]. Under certain conditions (see [22, 40, 41]) this wave collapses and transforms into a contracted ionisation wave, called a streamer, which has the form of a thin discharge filament. An analogous situation was recently simulated based on different sources of ionisation enhancement [20, 26, 28, 37, 38]. These results show how the very thin streamer emerges at first and subsequently expands (until it reaches the quasi-stationary state under given conditions). This very first phase of the early-stage streamer development remains experimentally unresolved. It is usually believed that pulsed corona discharges are the closest laboratory analogue for TLE streamers [11, 42] (although other approaches have been investigated as well, e.g. [43]). Such investigations have resulted in the quantification of the average magnitudes of crucial streamer parameters (velocity, diameter etc). However, the irreproducibility of such pulsed discharges and of the real TLE events hinders spectroscopic studies with high spatiotemporal resolution and makes any deeper analysis impossible. In particular, an understanding of the emergence of the streamer from the ionisation wave is experimentally based only on long-exposure imaging, see, e.g. [22]. As a result, the only information we have is the fact that at the moment of the emergence of the streamer its diameter is much lower than typically expected for the given conditions, compare the figures presented in [22, 40, 41] and recordings of real geophysical events [28, 37]. Early-stage streamers generated in dielectric barrier discharges are reproducible as well as stable [33, 44] even though the full development of the streamer is partially limited by Townsend scaling and the confinement of the discharge chamber.

The determination of the electric field in small-scale highly-transient plasmas is a challenging task, as direct measurements using laser spectroscopy still lack the necessary high-resolution and sensitivity [45]. Even though new methods have emerged [46, 47], the optical emission spectroscopy based method, as recently further developed by co-authors of this Letter [19, 33, 48–51], remains usually the only option. In this Letter, we present unique experimental results on expanding non-branching positive streamers in low pressure air. We present a detailed investigation of the very first moments of the initiation of the streamer, i.e. before the streamer achieves its quasi-stationary state. The investigated early-stage streamers are laboratory analogues to those present in the Blue Starters and Blue Jets observed in the lower stratosphere [52, 53]. We choose the volume barrier discharge setup in which reproducible and stable streamer events are generated periodically. This allows tracking the streamer initiation process from its very origin. We reveal an emerging streamer and describe its expansion by the experimentally determined electric field. This is the first experimental evidence of elementary streamer stages expressed quantitatively via the electric field with a resolution enabling a complete insight.

For the experiment, we selected the pressure of 1.3 kPa to imitate the mid-stratospheric conditions at an altitude of approximately 25 km. The discharge was generated in synthetic air between two electrodes (point anode and circle-shaped cathode, both covered by alumina dielectrics) with an inter-electrode gap of $d = 4$ cm, see figure 1 and in [33]. The barrier discharge electrode system was placed in vacuum inside a stainless steel chamber. The barrier discharge arrangement allowed the stabilisation of the occurrence of the streamer both temporally and spatially, which enabled a long-lasting accumulation of weak light emission of the streamer. A schematic drawing of the investigated discharge structure and the way it was radially scanned by a photomultiplier (PMT) is shown in figure 2. The optical emission was recorded by PMT (Hamamatsu H10721, rise-time of 570 ps)

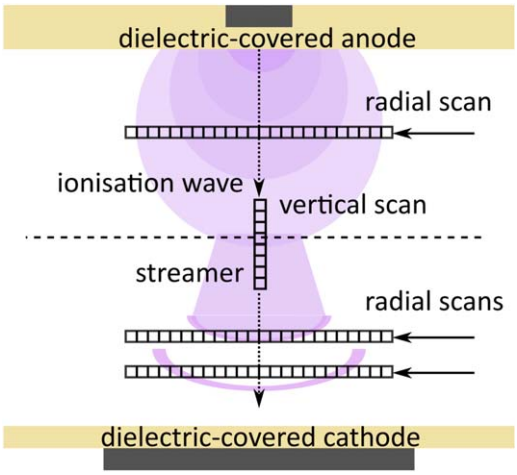

Figure 2. Schematic drawing of the DBD-electrode geometry, discharge pattern and the scanning procedures.

via 25 cm long capillary with an inner diameter of 1 mm. In order to record only spectrally selected emissions of the first negative and second positive system band, a set of suitable bandpass filters was applied. For the signal of the second positive system (SPS) with 0-0 vibrational transition, band head at 337.1 nm, a bandpass filter with FWHM of 9.7 nm was used (LOT Oriel 337FS10). For the 391.5 nm wavelength, a Semrock FF01-395/11 filter (central wavelength of 395 nm, FWHM 16.1 nm) was used, and for 370 nm, a Semrock FF01-370/10 filter (central wavelength 370 nm, FWHM 11.5 nm). The emission FNS waveform was corrected due to the overlap with the tail of the SPS (2, 5) band, which was done using spectra simulation as described in [33]. The recorded spectrally resolved waveforms were fitted and an Abel inversion procedure was applied to obtain the local intensity of the cylindrically symmetric discharge event.

In order to be able to trigger the streamer discharge with sufficient precision for an accurate PMT-scanning, a complex applied high-voltage waveform was used. Namely, an AC burst mode was employed with repetition frequency of 30 Hz. In the burst, two subsequent sine waveforms with a frequency of 1 kHz and amplitude of 3 kV were superimposed with a 500 ns long high-voltage pulse with an amplitude of 2.5 kV and rise time of 10 ns. The stability of the current and voltage waveforms was monitored using high-bandwidth current (Pearson 2877) and high-voltage (Tektronix P6015A) probes, respectively.

The measured applied voltage and the current in the external circuit are shown in figure 1. Three basic phases characteristic of the streamer discharge [20, 33] under given conditions can be identified: the primary ionisation and the formation of the diffuse (not contracted) ionisation wave is responsible for the first increase of the current. The subsequent rapid current rise tracks the positive streamer emergence and propagation. Lastly, as the streamer impacts onto the cathode dielectrics at approximately $t = 27$ ns, the transient conductive plasma channel is created. The fast deposition of the generated electric charge onto the dielectrics then quenches the discharge in the next 100 ns. In this Letter, the dynamics of the ionisation wave and mainly the early-stage streamer emergence and propagation (see also in figure 3) are studied in detail.

In figure 3(a), the vertical scan of the total discharge luminosity development is shown. The inter-electrode gap was scanned with steps of 1 mm by the high-speed photomultiplier, which was correlated with the applied voltage waveform. The above mentioned two important phases are denoted with coloured arrows. From the spatiotemporal development, the velocity of the diffuse ionisation wave, $1.5 \times 10^6\,\mathrm{m\,s^{-1}}$, and the velocity of the streamer, $1.5 \times 10^7\,\mathrm{m\,s^{-1}}$, were determined and are coherent with theoretically obtained values of the ionisation wave and early-stage streamer phenomena, see [26, 54].

Panel (b) of figure 3 shows the results of an electrical analysis of the current and voltage signals measured in an external circuit. The intrinsic electrical characteristics of the discharge plasma were inferred using methods presented in [33, 55]. The resulting development of the resistance of the plasma, of the effective electric field in the gap, and of the net transferred charge, are shown in figure 3(b). The resistance was computed from the following equation (see the analysis in [55]):

$$\varrho(t) = \frac{U_g(t)}{j_R(t)} = \frac{V(t) - Q(t)/C_d}{\left(1 - \frac{C_{\mathrm{cell}}}{C_d}\right)^{-1}\left(i(t) - C_{\mathrm{cell}}\frac{\mathrm{d}V(t)}{\mathrm{d}t}\right)}, \qquad (1)$$

where $j_R(t)$ is the net discharge current, $U_g(t)$ is the gap voltage, $i(t)$ is the measured current, $V(t)$ is the measured applied voltage in the external circuit, $Q(t)$ is the charge transferred in the external circuit, i.e. the integral of $i(t)$, while $C_{\mathrm{cell}} = 1.6$ pF and $C_d = 18$ pF are the effective capacitances of the discharge system determined by adopting the approach of Pipa *et al* [55].

Apparently, the resistance drops rapidly during the development of the first ionisation in the gap and subsequently also during the propagation of the streamer and its impact on the dielectric surface. In total, it drops by over three orders of magnitude. Within the first 40 ns, a charge of 20 nC is transferred through the gap (as shown in figure 3), finally it is 70 nC by the discharge in total. The ionisation wave transfers approximately 1.4 nC during the first 20 ns until its transformation into the early-stage streamer. This value corresponds to a number of electrons on the order of 10^9, which corresponds to a density of $2 \times 10^{15}\,\mathrm{m^{-3}}$ for the observed centimetre dimensions. Clearly, the criterion for streamer initiation is locally achieved under given conditions and the electron multiplication grows rapidly [20, 56]. At that moment, the diffuse ionisation wave becomes unstable and the early-stage streamer emerges. Between the 20th and 27th nanoseconds, the early-stage streamer generates a charge of 3.6 nC. The effective electric field in the gap $E_{\mathrm{eff}} = U_g(t)/d$ is expressed relatively to the threshold value E_k for which the air ionisation equals the electron attachment $\alpha = \eta$, i.e. $E_k = 120$ Td (i.e. $32\,\mathrm{kV\,cm^{-1}}$ at atmospheric pressure).

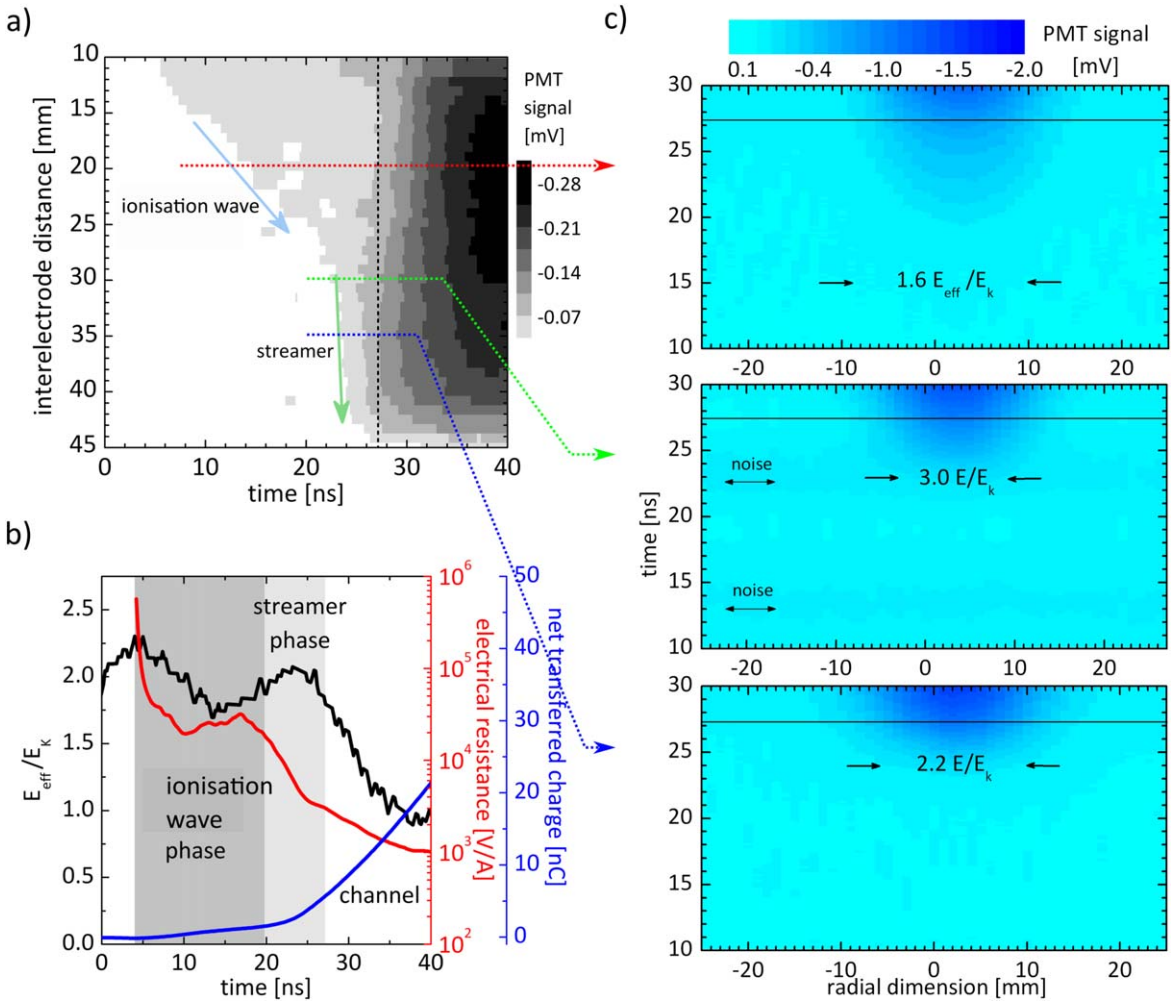

Figure 3. The axial (a) and radial (c) scans of the line-of-sight integrated discharge light emission as recorded with 570 ps resolution photomultiplier and sampled each 200 ps. In panel (b), the instantaneous development of the gas resistance (red), the effective electric field (black) and net transferred charge (blue) in the discharge are shown. The value of E_k is taken as 120 Td for given gas density at pressure 1.3 kPa (10 Torr) and temperature of 300 K. The arrows in panel (c) mark the front of the given ionisation event, wave (up) or streamer (middle, bottom). The repetition frequency of the high-voltage pulse, together with the sinusoidal waveform burst, was 30 Hz.

During the ionisation wave, the mean electric field in the gap reaches $E_{\mathrm{eff}} = 1.6\,E_k$. Note that this is a value determined from the electric measurement and therefore is an averaged value over the whole gap. The FNS emission at this coordinate was too weak compared with the SPS emission for a proper spectroscopic determination of the local electric field. Nevertheless, such a weak FNS intensity clearly provides complementary spectroscopic evidence of a very weak local E/N [48, 49].

In panel (c) of figure 3, the radial scans of the total discharge luminosity at three vertical coordinates y are shown. The arrow with the peak electric field value denotes the position of the ionisation wave front (15 ns, first radial scan) and the front of the streamer head (prior to and after the 23th nanoseconds at second and third scan, respectively) inferred from sub-nanosecond spectroscopy, see [19] and further in the text. The horizontal black line at approximately 27 ns denotes the moment of the impact of the streamer onto the cathode. It is apparent from the luminosity profiles at the denoted times that the ionisation wave, and later the streamer head, expands. The velocity of its radial expansion, in the range of $10^6\,\mathrm{m\,s^{-1}}$, is approximately one order of magnitude lower than the propagation velocity of the streamer head in the axial direction, as has been recently shown in [44]. Here both these velocities are also faster than in [44], which is caused by the more efficient photoionisation in the mixture with higher oxygen content [57] and lower pressure [58] in present case.

Using spectral band-pass filters, the spatially resolved emission waveforms of the emerging streamer event were recorded for selected nitrogen spectral bands. The line-of-sight radially resolved emission distribution was found to be Gaussian, and the process of Abel deconvolution described in [33, 59] was used to obtain the local emission of the streamer front. The radially resolved local emission intensities of the radiative states $N_2(C^3\Pi_u)$ (second positive system SPS with (0,0) vibronic transition at 337.1 nm) and $N_2^+(B^2\Sigma_u^+)$ (first negative system FNS with (0, 0) vibronic transition at 391.5 nm) were obtained from the corresponding line-of-sight waveforms The differential form of the ratio of these

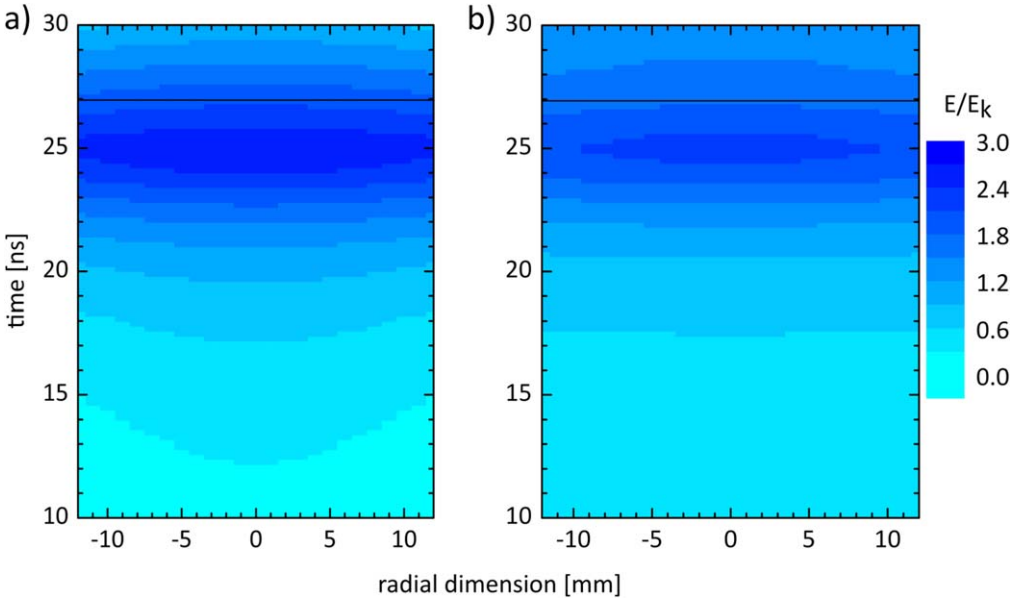

Figure 4. Determined electric field in the emerging (a) and subsequently expanding (b) streamer head. The enhanced local electric field is given with respect to $E_k = 120$ Td. The repetition frequency of the high-voltage pulse, together with the sinusoidal waveform burst, was 30 Hz in all presented experiments.

intensities is strongly dependent on the local electric field [9, 33, 48]:

$$\frac{\tau_{eff}^{\mathrm{FNS}} \cdot \mathrm{d}I_{\mathrm{FNS}}/\mathrm{d}t + I_{\mathrm{FNS}}}{\tau_{eff}^{\mathrm{SPS}} \cdot \mathrm{d}I_{\mathrm{SPS}}/\mathrm{d}t + I_{\mathrm{SPS}}} = R_{\mathrm{FNS/SPS}}(E/N), \tag{2}$$

where I_{FNS} and I_{SPS} denote the measured intensities of FNS and SPS, respectively, and $\tau_{\mathrm{eff}}^{\mathrm{FNS}} = 3.05$ ns and $\tau_{\mathrm{eff}}^{\mathrm{SPS}} = 20.54$ ns are the effective lifetimes for the pressure being considered which were obtained from the same constants as in [33]. The dependence $R_{\mathrm{FNS/\ SPS}}(E/N)$ was given by the following equation:

$$R_{\mathrm{FNS/SPS}}(E/N) = 0.5 \cdot 46 \cdot 0.065 \cdot \exp[-89(E/N)^{-0.5} - 402(E/N)^{-1.5}], \tag{3}$$

see [33, 48, 49]. The obtained spatiotemporal distributions of the reduced electric field strength for the emerging and for the expanding streamer are shown in figure 4. The determined electric field data were extrapolated to the lower field values (under the value of 15% of waveform maximum) by fitting the electric field waveform using the analytic expression presented by Kulikovsky in [60].

It is apparent from figure 4 that the curvature of the just emerged streamer head, panel (a), is smaller than in the case of the already expanded streamer, panel (b). Almost in 1 ns, the streamer becomes broader and the peak value of the electric field decreases by a factor of ~1.4. This is in agreement with the theoretical results of Luque *et al* [16] as well as with recent results of geophysical streamer simulations [37, 38]. Here, the peak value of the electric field decreases from almost $3E_k$ for the emerging streamer stage down to $2.2E_k$ for the expanding stage. We assume that the influence of the cathode charging by the approaching streamer head is negligible and so the streamer can be described as propagating in free space at the given coordinate.

Furthermore, to quantify the electron density, we have adopted the approach using the determined discharge current and local electric field (similarly to [61]). The fundamental parameter $n_e(t)$ was computed for the emerging streamer using the following equation:

$$n_e(t) = \frac{1}{e\mu_e(E(t))E(t)}\left(\frac{j_R(t)}{A} - \varepsilon_0\frac{\partial E(t)}{\partial t}\right), \tag{4}$$

where $\mu_e(E(t))$ is the local electron mobility dependent on the temporally changing electric field, $j_R(t)$ is the net discharge current, and A is the local cross-sectional area of the filament given by its diameter, which was obtained from measurements similar to those presented in figure 3(c). This one-dimensional approach may overestimate $n_e(t)$ under the given conditions. The dependence of the electron mobility on the determined electric fields was computed using the two-term approximation to the solution of the Boltzmann equation and the Biagi cross-sections [62, 63]. Furthermore, the development of the mean electron energy was determined from the same computations.

The results for the streamer-initiated electron ensemble parameters are shown in figure 5. After the 20th nanosecond, the current is rising rapidly. Due to the positive value of $\partial E/\partial t$, the resulting increase in the electron density is a bit decelerated (see equation (4)), but finally reaches the value of $1 \times 10^{16}\,\mathrm{m}^{-3}$ at the moment of the maximum value of the electric field, i.e. in the streamer head. Subsequently, as the current rise decelerates, the further growth of the electron density is almost stopped at 26 ns. Later on, the term $\partial E/\partial t$ gets smaller and even negative and so the rise of the electron density starts again, increasing almost one order of magnitude in the next several nanoseconds. The values found are in good

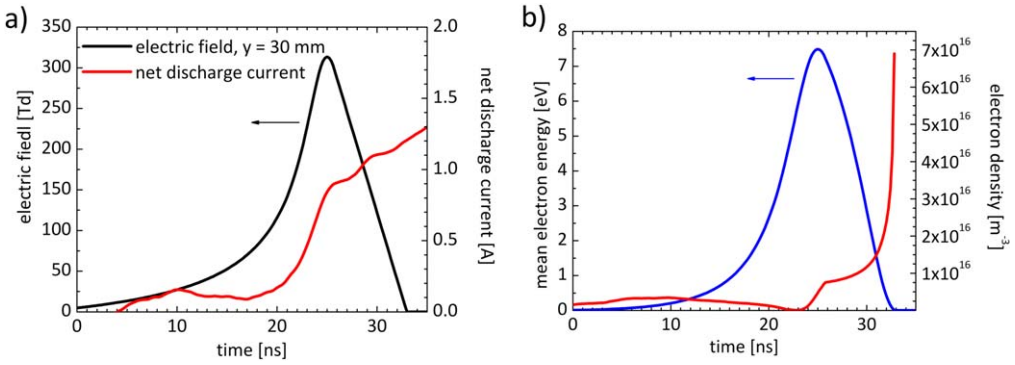

Figure 5. Instantaneous development of the electric field, net discharge current (a), mean electron energy and electron density according to equation (4), see panel (b).

agreement with the Townsend scaling (for electron density with $\sim N^2$, where N is the air particle density) and with the theoretically obtained values in [54]. The maximum mean electron energy reaches 7.5 eV.

In conclusion, we have reported unique results of an experimental determination of the basic plasma parameters of a streamer head in the early stages of its development—when it emerges from the ionisation wave and further expands. We have quantified the radial development of the electric field, electron density, and the streamer acceleration in the axial as well as the radial direction with sub-nanosecond resolution. Our results confirm the outcomes of numerical predictions [16]. It is worth noting that these results bear a striking similarity to the numerically obtained results of streamer emergence from ionisation waves reported in [26, 28, 37, 38], yet under different pressures.

In addition, the results in this Letter have an important methodological consequence. The spectrally resolved imaging of accidentally appearing lightning events is practically the only method for obtaining spatially and temporally resolved information about lightning or TLEs streamers [64–67]. As a consequence, a detailed experimental spectroscopic understanding of the TLE streamer analogues has to be obtained primarily under laboratory conditions [7, 33, 64] as has been proposed here for the streamer analogue of a Blue Starter and Jet. In this Letter we have taken an essential step towards revealing the microphysics of the emerging streamers on their ultra-short characteristic time-scales under conditions of pressure relevant for the TLEs. The approach presented for the determination of the electric field from sub-nanosecond recording is important not only for the investigation of atmospheric electricity phenomena at the ground level, but also for investigations carried out with balloons or satellites. The appropriately equipped ASIM [68] and TARANIS [69] space-missions of the European Space Agency and the French Space Agency, respectively, will provide new insights into the fundamental physics of lightning and TLEs. The space-mission data [70] might be analysed in the light of laboratory benchmark experiments trying to mimic specific aspects of those phenomena, as has been presented in this Letter.

Acknowledgments

This research was funded by the Academy of Sciences of the Czech Republic under project M100431201. TH was supported by the European Science Foundation Research Networking Programme TEA-IS (ex-change Grant No. 4219). ZB was supported by the Czech Science Foundation, project No. 15-04023S. FJGV was supported by the Spanish Ministry of Science and Innovation (MINECO) under project ESP2017-86263-C4-4-R. TH is grateful for the support of project LM2018097 funded by the Ministry of Education, Youth and Sports of the Czech Republic.

ORCID iDs

T Hoder https://orcid.org/0000-0001-5346-6275
Z Bonaventura https://orcid.org/0000-0002-9591-6040
M Šimek https://orcid.org/0000-0003-1730-8493

References

[1] Raether H 1939 *Z. Phys.* **112** 464–89
[2] Loeb L B 1948 *Phys. Rev.* **74** 210–2
[3] Meek J M 1940 *Phys. Rev.* **57** 722–8
[4] Marode E, Djermoune D, Dessante P, Deniset C, Ségur P, Bastien F, Bourdon A and Laux C 2009 *Plasma Phys. Control. Fusion* **51** 124002
[5] Naidis G V, Tarasenko V F, Babaeva N Y and Lomaev M I 2018 *Plasma Sources Sci. Technol.* **27** 013001
[6] Černák M, Hoder T and Bonaventura Z 2019 *Plasma Sources Sci. Technol.* **29** 013001
[7] Šimek M and Bonaventura Z 2018 *J. Phys. D: Appl. Phys.* **51** 504004
[8] Kogelschatz U 2004 *Plasma Phys. Control. Fusion* **46** B63
[9] Hoder T, Černák M, Paillol J, Loffhagen D and Brandenburg R 2012 *Phys. Rev.* E **86** 055401
[10] Pasko V P 2010 *J. Geophys. Res.: Space Phys.* **115** A00E35
[11] Pasko V P 2007 *Plasma Sources Sci. Technol.* **16** S13–29
[12] Gordillo-Vázquez F J 2008 *J. Phys. D: Appl. Phys.* **41** 234016
[13] Pasko V P 2008 *Plasma Phys. Control. Fusion* **50** 124050
[14] Winkler H and Notholt J 2015 *J. Atmos. Sol. Terr. Phys.* **122** 75–85

[15] Černák M, Kováčik D, Ráhel J, Stahel P, Zahoranová A, Kubincová J, Tóth A and Černáková L 2011 *Plasma Phys. Control. Fusion* **53** 124031
[16] Luque A, Ratushnaya V and Ebert U 2008 *J. Phys. D: Appl. Phys.* **41** 234005
[17] Naidis G V 2009 *Phys. Rev.* E **79** 057401
[18] Bonaventura Z, Bourdon A, Celestin S and Pasko V P 2011 *Plasma Sources Sci. Technol.* **20** 035012
[19] Hoder T, Bonaventura Z, Bourdon A and Šimek M 2015 *J. Appl. Phys.* **117** 073302
[20] Yurgelenas Y V and Wagner H E 2006 *J. Phys. D: Appl. Phys.* **39** 4031–43
[21] Kozlov K V and Wagner H E 2007 *Contrib. Plasma Phys.* **47** 26–33
[22] Clevis T T J, Nijdam S and Ebert U 2012 *J. Phys. D: Appl. Phys.* **46** 045202
[23] Inada Y, Aono K, Ono R, Kumada A, Hidaka K and Maeyama M 2017 *J. Phys. D: Appl. Phys.* **50** 174005
[24] Wilson C T R 1924 *Proc. Phys. Soc. London* **37** 32D–37D
[25] Franz R C, Nemzek R J and Winckler J R 1990 *Science* **249** 48–51
[26] Luque A and Ebert U 2009 *Nat. Geosci.* **2** 757
[27] Qin J, Celestin S and Pasko V P 2011 *J. Geophys. Res.: Space Phys.* **116** A06305
[28] Qin J, Pasko V P, McHarg M G and Stenbaek-Nielsen H C 2014 *Nat. Commun.* **5** 3740
[29] Celestin S and Pasko V P 2010 *Geophys. Res. Lett.* **37** L07804
[30] Luque A, Ebert U and Hundsdorfer W 2008 *Phys. Rev. Lett.* **101** 075005
[31] Kuo C L *et al* 2009 *J. Geophys. Res.: Space Phys.* **114** A04314
[32] Wagenaars E, Bowden M D and Kroesen G M W 2007 *Phys. Rev. Lett.* **98** 075002
[33] Hoder T, Šimek M, Bonaventura Z, Prukner V and Gordillo-Vázquez F J 2016 *Plasma Sources Sci. Technol.* **25** 045021
[34] Liu N, Kosar B, Sadighi S, Dwyer J R and Rassoul H K 2012 *Phys. Rev. Lett.* **109** 025002
[35] Pechereau F, Bonaventura Z and Bourdon A 2016 *Plasma Sources Sci. Technol.* **25** 044004
[36] Dubinova A, Rutjes C, Ebert U, Buitink S, Scholten O and Trinh G T N 2015 *Phys. Rev. Lett.* **115** 015002
[37] Liu N, Dwyer J R, Stenbaek-Nielsen H C and McHarg M G 2015 *Nat. Commun.* **6** 7540
[38] Liu N, Boggs L D and Cummer S A 2016 *Geophys. Res. Lett.* **43** 2365–73
[39] Sorokin D A, Tarasenko V F, Beloplotov D V and Lomaev M I 2019 *J. Appl. Phys.* **125** 143301
[40] Briels T M P, van Veldhuizen E M and Ebert U 2008 *IEEE Trans. Plasma Sci.* **36** 908–9
[41] Briels T M P, van Veldhuizen E M and Ebert U 2008 *J. Phys. D: Appl. Phys.* **41** 234008
[42] Ebert U, Nijdam S, Li C, Luque A, Briels T and van Veldhuizen E 2010 *J. Geophys. Res.: Space Phys.* **115** A00E43
[43] Sosnin E A, Naidis G V, Tarasenko V F, Skakun V S, Panarin V A, Babaeva N Y, Baksht E K and Kuznetsov V S 2018 *Phys. Plasmas* **25** 083513
[44] Höft H, Becker M M and Kettlitz M 2018 *Plasma Sources Sci. Technol.* **27** 03LT01
[45] Böhm P, Kettlitz M, Brandenburg R, Höft H and Czarnetzki U 2016 *Plasma Sources Sci. Technol.* **25** 054002
[46] Dogariu A, Goldberg B M, O'Byrne S and Miles R B 2017 *Phys. Rev. Appl.* **7** 024024
[47] Chng T L, Orel I S, Starikovskaia S M and Adamovich I V 2019 *Plasma Sources Sci. Technol.* **28** 045004
[48] Obrusník A, Bílek P, Hoder T, Šimek M and Bonaventura Z 2018 *Plasma Sources Sci. Technol.* **27** 085013
[49] Bílek P, Obrusník A, Hoder T, Šimek M and Bonaventura Z 2018 *Plasma Sources Sci. Technol.* **27** 085012
[50] Hoder T, Synek P, Chorvat D, Rahel J, Brandenburg R and Cernak M 2017 *Plasma Phys. Control. Fusion* **59** 074001
[51] Bílek P, Šimek M and Bonaventura Z 2019 *Plasma Sources Sci. Technol.* **28** 115011
[52] Wescott E M, Sentman D D, Heavner M J, Hampton D L, Osborne D L and Vaughan O H Jr 1996 *Geophys. Res. Lett.* **23** 2153–6
[53] Wescott E M, Sentman D D, Stenbaek-Nielsen H C, Huet P, Heavner M J and Moudry D R 2001 *J. Geophys. Res.: Space Phys.* **106** 21549–54
[54] Liu N and Pasko V P 2004 *J. Geophys. Res.: Space Phys.* **109** 04301
[55] Pipa A V, Koskulics J, Brandenburg R and Hoder T 2012 *Rev. Sci. Instrum.* **83** 115112
[56] Rabie M and Franck C M 2016 *J. Phys. D: Appl. Phys.* **49** 175202
[57] Wormeester G, Pancheshnyi S, Luque A, Nijdam S and Ebert U 2010 *J. Phys. D: Appl. Phys.* **43** 505201
[58] Pancheshnyi S, Nudnova M and Starikovskii A 2005 *Phys. Rev.* E **71** 016407
[59] Šimek M and Ambrico P F 2012 *Plasma Sources Sci. Technol.* **21** 055014
[60] Kulikovsky A A 1998 *Phys. Rev.* E **57** 7066–74
[61] Donko Z, Schulze J, Mueller S and Czarnetzki U 2011 *Appl. Phys. Lett.* **98** 251502
[62] Hagelaar G J M and Pitchford L C 2005 *Plasma Sources Sci. Technol.* **14** 722–33
[63] BOLSIG+ solver ver 03/2016 Biagi database (N_2,O_2) www.lxcat.net; Accessed: 6 April, 2017
[64] Šimek M 2014 *J. Phys. D: Appl. Phys.* **47** 463001
[65] Gordillo-Vázquez F J, Passas M, Luque A, Sánchez J, van der Velde O A and Montanyá J 2018 *J. Geophys. Res.: Atmos.* **123** 2336–46
[66] Kanmae T, Stenbaek-Nielsen H C and McHarg M G 2007 *Geophys. Res. Lett.* **34** L07810
[67] Ihaddadene M A and Celestin S 2017 *J. Geophys. Res.: Space Phys.* **122** 1000–14
[68] Neubert T, Østgaard N, Reglero V, Blanc E, Chanrion O, Oxborrow C A, Orr A, Tacconi M, Hartnack O and Bhanderi D D V 2019 *Space Sci. Rev.* **215** 26
[69] Lefeuvre F, Blanc E, Pinçon J L, Roussel-Dupré R, Lawrence D, Sauvaud J A, Rauch J L, de Feraudy H and Lagoutte D 2008 *Space Sci. Rev.* **137** 301–15
[70] Neubert T *et al* 2020 *Science* **367** 183–6